



## Sustaining charge-neutral or charged supercurrents in excitonic Josephson junctions based on graphene heterostructures

Chuanyi Zhang <sup>1,2</sup>, Weifeng Zhang,<sup>1</sup> Yu Jia,<sup>1,3</sup> and Zhenyu Zhang <sup>2,\*</sup>

<sup>1</sup>Center for Topological Functional Materials, Henan Key Laboratory of Photovoltaic Materials, Henan University, Kaifeng 475004, China

<sup>2</sup>International Center for Quantum Design of Functional Materials (ICQD), Hefei National Laboratory for Physical Sciences at Microscale, and Synergetic Innovation Center of Quantum Information and Quantum Physics, University of Science and Technology of China, Hefei 230026, China

<sup>3</sup>School of Physics and Engineering, Zhengzhou University, Zhengzhou 450001, China



(Received 5 January 2021; revised 7 October 2021; accepted 8 November 2021; published 30 November 2021)

In a Josephson junction between two exciton condensates, the tunneling of charge-neutral electron-hole pairs has gained primary attention in the form of a supercurrent, which otherwise is challenging to detect experimentally. Here we design excitonic Josephson junctions based on graphene heterostructures that allow us to selectively sustain charge-neutral or charged supercurrent, offering unprecedented opportunities for revealing exotic physics of exciton condensates. In our schemes, each exciton condensate consists of a graphene monolayer vertically coupled with another graphene monolayer (GML), bilayer, or trilayer, shown to have characteristically different quantum phase transition temperatures. When two such identical condensates are connected, a neutral supercurrent always dominates within the GML/GML scheme, while in the other two schemes, a carrier-density induced transition can take place between the neutral and charged supercurrents. More strikingly, in the charged regime, both the electron or hole dominance and the DC or AC nature can be tuned by the chemical potential differences of the junction. These findings are also expected to be applicable to excitonic Josephson junctions beyond the graphene-based architecture.

DOI: [10.1103/PhysRevB.104.195309](https://doi.org/10.1103/PhysRevB.104.195309)

### I. INTRODUCTION

Exciton is an important elementary excitation in a semiconductor, typically referring to an electron and its hole counterpart mediated by the Coulomb attraction in the conduction and valence bands, respectively. In the low density and low temperature regime, there emerges a macroscopically coherent state of a collection of excitons, namely, an exciton condensate [1], which is a particularly appealing quantum state of matter that may harbor room-temperature superconductivity [2] and other exotic properties [3–6]. The realization of exciton condensation has stimulated much experimental effort [7–11]. As a compelling example, the macroscopic coherent nature of an exciton condensate in forming interference patterns has been definitively demonstrated [12]. Furthermore, two such exciton condensates can be separated by a barrier to behave as an excitonic Josephson junction, which serves as a powerful platform for exploring various manifestations of the macroscopic quantum phenomena [13–19]. It is therefore conceptually fruitful to study supercurrents in excitonic Josephson junctions under diverse physical conditions.

To date, attention has been primarily paid to the electron-hole (e-h) pair tunneling in evaluating the Josephson current, largely based on semiconductor quantum wells [13–16]. In these systems, the supercurrent is inherently charge neutral, and owing to the strong attractive Coulomb interaction

between electrons and holes, e-h recombination may take place in the barrier, which in turn will impede exact determination of the supercurrent. As increasing branches of the two-dimensional (2D) materials family have been discovered more recently [20–25], their unique electron properties have also been explored for potential realization of exciton condensation [26–35], even at high temperatures [36]. These exciting advances naturally offer superior schemes of excitonic Josephson junctions with unprecedented properties and performance at atomic scale precision.

In this work we design excitonic Josephson junctions based on graphene heterostructures that allow us to selectively sustain charge-neutral or charged supercurrent, offering unprecedented opportunities for revealing exotic physics of exciton condensates. In our schemes, each exciton condensate consists of a graphene monolayer vertically coupled with another graphene monolayer (GML), bilayer (GBL), or trilayer (GTL), shown to have characteristically different quantum phase transition temperatures of Berezinskii-Kosterlitz-Thouless (BKT) and Bardeen-Cooper-Schrieffer (BCS). When two such identical condensates are connected, a neutral supercurrent is shown to always dominate within the GML/GML scheme, while in the other two schemes, a carrier-density induced transition can take place between the neutral and charged supercurrents. More strikingly, in the charged regime, both the electron or hole dominance and the DC or AC nature can be fine tuned by the chemical potential differences of the junction. These findings are also expected to be applicable to other excitonic Josephson junctions

\*Corresponding author: zhangzy@ustc.edu.cn

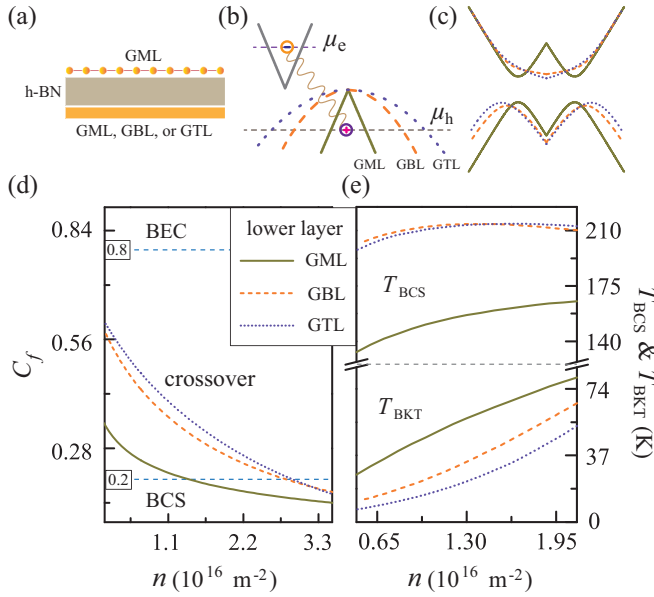


FIG. 1. (a) Schematic diagram of two double layer structure separated by a few-layer hexagonal boron nitride (h-BN) film. The upper layer is GML, and the lower layer can be a GML, GBL, or GTL. (b) Dispersion relations for electrons and holes in the upper and lower layers without the interlayer Coulomb interaction. (c) Gapped band dispersions in the exciton insulator regime due to the interlayer Coulomb interaction. (d) The condensate fraction as a function of the carrier density at 1 K. (e) Variation of the BCS critical condensation temperature and BKT transition temperature with the carrier density for different hole dispersion relations.

involving 2D materials beyond graphene. The paper is organized as follows: In Sec. II the exciton condensation is studied with the Bogoliubov–de Gennes Hamiltonian in the graphene heterostructures [Fig. 1(a)]. In Sec. III the phase transitions are discussed for different physical parameters, and the corresponding transition temperatures are given. In the coherent regime, the excitonic Josephson effect is investigated, including charge-neutral or charged supercurrents. Finally, this work is summarized in Sec. IV.

## II. THEORETICAL MODEL

Before constructing an excitonic Josephson junction, we first study a constituent exciton condensate involving double-layer structure based on graphene, as represented in Fig. 1(a). The two layers are separated by a hexagonal boron nitride (h-BN) film with about 5 nm in thickness. Given the weak coupling between the upper and lower graphene layers [37–39], we can neglect interlayer tunneling in such devices. Exciton condensation constitutes of indirect excitons, namely, the electrons and holes reside in the upper and lower layers, respectively.

For different hole dispersion relations, the Bogoliubov–de Gennes Hamiltonian of the systems has the following universal structure:

$$\mathcal{H}_{\text{BDG}}(\mathbf{k}) = \begin{pmatrix} \xi_e(\mathbf{k}) & \Delta(\mathbf{k}) \\ \Delta^\dagger(\mathbf{k}) & -\xi_h(\mathbf{k}) \end{pmatrix}, \quad (1)$$

where the terms  $\xi_e(\mathbf{k})$  and  $\xi_h(\mathbf{k})$  describe the energy of electrons and holes, respectively, which for convenience include the corresponding chemical potentials  $\mu_e$  and  $\mu_h$ .  $\Delta(\mathbf{k}, \beta)$  is the order parameter and expressed as  $-\sum_{\mathbf{k}'} g_{\mathbf{k}-\mathbf{k}'} \Delta(\mathbf{k}') [1 - f^+(\mathbf{k}') - f^-(\mathbf{k}')]/2E(\mathbf{k}')$ , with  $g_{\mathbf{k}-\mathbf{k}'}$  being the Coulomb interaction. Here  $E(\mathbf{k}) = \sqrt{(\xi_e + \xi_h)^2/4 + \Delta^2}$ , and the distribution function has the form  $f^{+(-)}(\mathbf{k}) = 1/(\exp\{\beta[E(\mathbf{k}) + (-)(\xi_e - \xi_h)/2]\} + 1)$ , with  $\beta$  the inverse temperature.

The densities of electrons and holes can be independently tuned by the electrostatic gates in the upper and lower graphene layers, respectively. For optimal exciton condensation, we concentrate on the cases with the same densities of electrons and holes here, such that both the Fulde-Ferrell-Larkin-Ovchinnikov and Sarma phases will not appear [40,41]. Near the Fermi surfaces of the two layers, electrons of wave vector  $\mathbf{k}$  interact with holes of  $-\mathbf{k}$  through the Coulomb attraction. At sufficiently low carrier densities and low temperature, an energy gap appears, as shown in Fig. 1(c), which can decrease the total energy of the system, resulting in the exciton insulator phase [26,28,29,35]. Such interlayer couplings alter the band dispersions illustrated in Fig. 1(b) to those shown in Fig. 1(c), displaying the distinct existence of the energy gaps in the heterostructures. Accordingly, the relativistic Dirac nature of electrons or holes in pristine graphene is destroyed, and the systems are immune to the Klein paradox [42–44]. Such a qualitative picture is also consistent with related experimental observations in graphene-based heterostructures [37,38].

Due to the existence of the two equivalent but independent sublattices in the unit cell of graphene, the pseudospin degrees of freedom emerge in the momentum space, and the massless Dirac description of the low-energy states originates from the coexistence of the orbital motion and pseudospins near the high-symmetry points  $\mathbf{K}$  and  $\mathbf{K}'$ . The order parameter of exciton condensation can be determined self-consistently by the chemical potential  $\mu$ , with explicit consideration of the fourfold spin and valley degeneracy, as well as pseudospins in graphene. In addition, the screened Coulomb interaction associated with the electrostatic gates may have some effect on the exciton energy [45], but given by the indirect nature of the excitons, such effects are very limited, especially in the tunneling regime between exciton condensates with comparable densities (see Appendix A).

## III. RESULTS AND DISCUSSION

### A. Exciton condensation

At a given and sufficiently low temperature, as the carrier density varies from high to low, the system approaches the exciton condensation from the e-h plasma [46], defining a critical density. Below this density, the system is in the BCS state in the form of exciton insulators [47]. When the density is further lowered, the system enters the BEC state, characterized by a macroscopically correlated Boson condensate [34]. The transition from the BCS to BEC state is continuous upon decreasing the density. We introduce the condensate fraction  $C_f$  to measure the degree of condensation, which can be expressed as  $C_f = \sum_{\mathbf{k}} \{u^2(\mathbf{k})v^2(\mathbf{k})[1 - f^+(\mathbf{k}) - f^-(\mathbf{k})]^2\} / \sum_{\mathbf{k}} \{u^2(\mathbf{k})f^+(\mathbf{k}) + v^2(\mathbf{k})[1 - f^-(\mathbf{k})]\}$ , with  $v^2 = 1 - u^2 = [1 - (\xi_e + \xi_h)/2E]/2$ . As indicated in Fig. 1(d), it is generally

adopted that the BEC state appears when  $C_f > 0.8$ , the BCS state arises when  $C_f < 0.2$ , while the intermediate range corresponds to the BEC-BCS crossover region with coexistence of BEC and BCS features [34,48]. From Fig. 1(d), obtained at the temperature 1 K, we can see that the condensate fraction is affected by the different hole dispersion relations, and the transition density from the BCS state to the crossover regime is higher when the GBL or GTL is used in the lower layer. The underlying reason can be attributed to the stronger binding energy of excitons when heavier holes are involved. In addition,  $C_f$  increases much more rapidly at low carrier densities.

In Fig. 1(e) we also illustrate how the BCS and BKT temperatures  $T_{\text{BCS}}$  and  $T_{\text{BKT}}$  sensitively depend on the carrier density for the three different systems, in particular, the dramatic increases in  $T_{\text{BCS}}$  and significant decreases in  $T_{\text{BKT}}$  when adopting GBL or GTL in the lower layer. When the temperature is lower than  $T_{\text{BCS}}$ , we get nonzero  $\Delta(\mathbf{k}, \beta)$ , but it only signifies the emergence of isolated condensation droplets, lacking macroscopic phase coherence among the droplets. A coherent condensate emerges when the temperature is lower than  $T_{\text{BKT}}$  [49]. The value of  $T_{\text{BCS}}$  is obtained when  $\max[\Delta(\mathbf{k}, \beta)] \rightarrow 0$ . To quantify  $T_{\text{BKT}}$ , we first get the superfluid weight  $W_{\text{sf}}$ , which further satisfies the universal relation  $T_{\text{BKT}} = \pi W_{\text{sf}}(1/T_{\text{BKT}}, n)/8$  [50]. In doing so, a slowly varying vector gauge potential is introduced into the Hamiltonian, which is then expanded up to the quadratic order of the gauge potential. The current-current response function is obtained from linear response theory [51–53], and  $W_{\text{sf}}$  is expressed in long wavelength limit as

$$W_{\text{sf}}(\beta, n) = \sum_{k,j,l} \frac{f(E_l) - f(E_j)}{E_j - E_l} (\langle \psi_j | \partial_k \mathcal{H} | \psi_l \rangle \langle \psi_l | \partial_k \mathcal{H} | \psi_j \rangle - \langle \psi_j | \partial_k \mathcal{H} \sigma_z | \psi_l \rangle \langle \psi_l | \partial_k \mathcal{H} \sigma_z | \psi_j \rangle), \quad (2)$$

where  $\psi_j$  is the eigenvector of the Hamiltonian with eigenvalue  $E_j$ , and  $\sigma_z$  is the Pauli matrix acting in the Nambu space. The first term in the parentheses of Eq. (2) is the diamagnetic term, which reflects the static Meissner effect in exciton superfluid, while the second one is the paramagnetic term.

To comprehend the variation of  $T_{\text{BCS}}$  and  $T_{\text{BKT}}$  in Fig. 1(e) with different carrier densities, we draw attention to the carrier effective mass. When GML, GBL, or GTL is applied in the lower layer, the hole effective mass becomes heavier sequentially at a given carrier density. The hole effective mass differences translate into different partitions of electrons and holes in a given exciton of the systems, which further result in different superfluid weights at a given temperature. Specifically, whereas  $T_{\text{BCS}}$  is much higher when heavier holes are involved for a given carrier density, the corresponding  $T_{\text{BKT}}$  is lower and increases with the carrier density. Experimentally, delicate transport measurements such as in the Coulomb drag approach can be employed to detect the anomalous signatures when the temperature approaches  $T_{\text{BCS}}$ , for instance, the drag resistivity should show a pronounced upturn, caused by the dramatic electron-hole pair fluctuations at the transition [54,55].

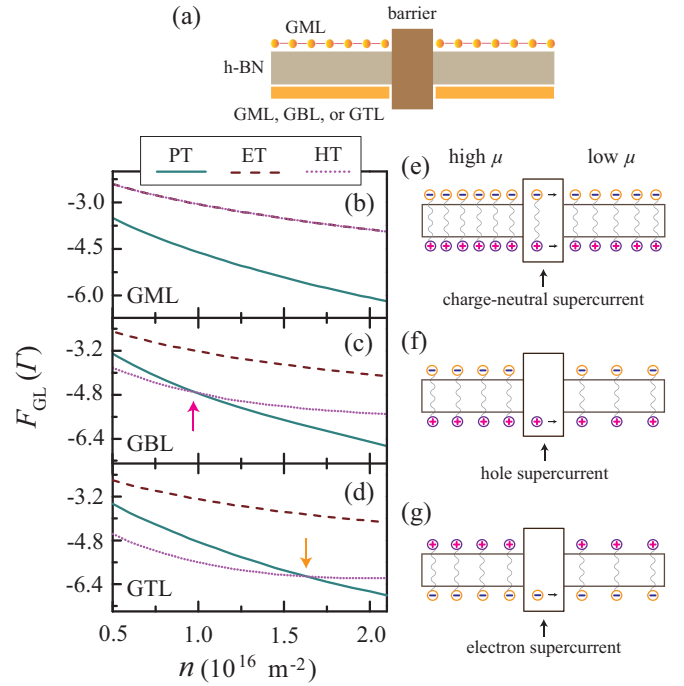


FIG. 2. (a) Schematic diagram of the excitonic Josephson junction with two identical condensates separated by a barrier. (b)–(d) The Ginzburg-Landau free energy for e-h pair tunneling (PT), electron tunneling (ET), and hole tunneling (HT) as functions of the carrier density when the lower layer is, respectively, a GML, GBL, or GTL. (e)–(g) Schematic diagrams of the dominant charge-neutral, hole, or electron tunneling supercurrent regimes, with the condensates formed between the GML and GBL or GTL.

## B. Excitonic Josephson effect

Given the prerequisites on the characteristic phase transitions of the exciton condensates in the double-layer structures, we now can proceed to excitonic Josephson junctions formed by two identical condensates separated by a barrier, as illustrated in Fig. 2(a). In a conventional superconducting Josephson junction [56], the tunneling of Cooper pairs dominates the anomalous supercurrent, and the Ginzburg-Landau free energy containing the tunneling term is minimized [57,58]. Here we adopt this method to discuss the tunneling regime of the excitonic Josephson junctions, and investigate the nature of the dominant supercurrent under different junction designs.

For the present systems, the Ginzburg-Landau free energy has the expression  $F_{\text{GL}} = -\text{Tr} \ln(1 - G_L T G_R T)/\beta$ , where  $G_{L(R)}$  is the Green function of the left (right) condensate given by  $G = 1/[i\omega_n - \mathcal{H}_{\text{BDG}}(\mathbf{k})]$ , with  $\omega_n$  being the fermionic Matsubara frequency. The tunneling matrix  $T$  is expressed as  $\begin{pmatrix} \Gamma_{kk'} & 0 \\ 0 & \Gamma_{kk'} \end{pmatrix}$  for the e-h pair tunneling [14],  $\begin{pmatrix} \Gamma_{kk'} & 0 \\ 0 & 0 \end{pmatrix}$  for the electron tunneling, and  $\begin{pmatrix} 0 & 0 \\ 0 & \Gamma_{kk'} \end{pmatrix}$  for the hole tunneling, which have different forms in the junction with two exciton condensates separated by a normal conductor [59]. Here  $\Gamma_{kk'}$  is the tunneling matrix element, and can be assumed to be independent of the wave vectors if the carrier energies involved are low.

In our further discussions, for convenience the carrier density in the left condensate is assumed to be slightly higher than that in the right condensate. For given carrier densities, the temperature of the setup should be even lower than the lower  $T_{\text{BKT}}$  of the two constituent condensates, to ensure macroscopic phase coherence in the whole system. In this case, the macroscopic wave functions overlap in the tunneling barrier, inducing the Josephson effect. The free energy  $F_{\text{GL}}$  can be calculated for different particle densities. As shown in Fig. 2(b), when GML is utilized in the lower layer,  $F_{\text{GL}}$  for the e-h pair tunneling is minimal for arbitrary carrier density, and accordingly dominates the Josephson current. Furthermore, in this scheme, the same free energies are obtained for the electron tunneling and hole tunneling, which reflects the same partitions of electron and hole in the pair condensation. Here we note that, although the linear dispersion relations are used for electron and hole, the results can be extended to other cases as well, namely, as long as there exists the particle-hole symmetry, the pair tunneling will always dominate at a given carrier density, as seen in the conventional superconducting Josephson junctions.

When a GBL is used in the lower layer to increase the hole effective mass, the electron and hole partitions are unequal in the pair. In this case, the free energy for hole tunneling is the lowest at  $n < 10^{16} \text{ m}^{-2}$ , while  $F_{\text{GL}}$  for pair tunneling is minimal at  $n > 10^{16} \text{ m}^{-2}$ , defining a critical carrier density  $n_c = 10^{16} \text{ m}^{-2}$ . If the hole effective mass increases further to the case when a GTL is applied in the lower layer, the qualitatively similar phenomena are found, but a higher critical density,  $n_c \approx 1.6 \times 10^{16} \text{ m}^{-2}$ . From Figs. 2(c) and 2(d) we see that the critical carrier densities for both schemes are located in the BEC-BCS crossover regime indicated in Fig. 1(d). In addition, when a GBL or GTL is used, the free energy of electron tunneling is always much higher than that of the e-h pair tunneling or hole tunneling as the carrier density varies.

More generally, we present an analytic expression to determine the crossover density, separating the dominant hole tunneling and e-h pair tunneling regimes, and the discriminant  $\Pi_h$  has the form at a temperature approaching 0 K (see Appendix B),

$$\Pi_h = \sum_{kk'\kappa} \frac{(-1)^{\kappa+1} X_{L\kappa} X_{R(3-\kappa)} [X_{L\kappa} X_{R(3-\kappa)} + 2Y_{L\kappa} Y_{R(3-\kappa)}]}{E_{R(3-\kappa)} - E_{L\kappa}}, \quad (3)$$

where  $(X_{Y\kappa}^{\kappa})$  is the wave function of Eq. (1) with the eigenvalue  $E_{Y\kappa}$ ,  $\iota = L$  or  $R$ , represents the left and or right condensate, and  $\kappa = 1, 2$  for the upper and lower eigenvalues, respectively. The summation over the wave vectors is operated for  $\mathbf{k}$  in the left condensate and for  $\mathbf{k}'$  in the right. With this criterion, it is clear that the hole tunneling dominates if  $\Pi_h > 0$ , corresponding to very large partition differences between electrons and holes in the pairs, while for  $\Pi_h < 0$ , the partition differences are small, and the e-h pair tunneling becomes predominant. At  $n = n_c$ , i.e.,  $\Pi_h = 0$ , defining the crossover point. These analytical results agree well with those in the right panel of Fig. 2.

In the above discussion, the electron tunneling is always suppressed by varying the carrier density, and how to realize

it as the main tunneling regime is an interesting issue. To achieve this goal, we take an effective approach, namely, by modulating the chemical potentials with electrons and holes residing in the lower and upper layers, respectively. With the same procedure utilized in Eq. (3), another criterion is derived to define the transition from the e-h pair to electron tunneling or vice versa, and the corresponding discriminant,

$$\Pi_e = \sum_{kk'\kappa} \frac{(-1)^{\kappa+1} Y_{L\kappa} Y_{R(3-\kappa)} [Y_{L\kappa} Y_{R(3-\kappa)} + 2X_{L\kappa} X_{R(3-\kappa)}]}{E_{R(3-\kappa)} - E_{L\kappa}}. \quad (4)$$

As expected, there also exists a crossover density separating the dominant electron tunneling ( $\Pi_e > 0$ ) and the e-h pair tunneling regimes ( $\Pi_e < 0$ ).

In practice, different tunneling regimes will result in different kinds of excitonic Josephson current to be detected experimentally. When the pair tunneling dominates in the Josephson junction, it will cause an electron current in one layer and an equal hole current in the other layer in the same direction, so there is charge-neutral supercurrent flowing through the barrier [see Fig. 2(e)]. In this case, this supercurrent can be direct or alternating, determined by the chemical potential difference between the two exciton condensates [19]. When the single particle tunneling is dominant, regardless of electron or hole tunneling, there will exist a charged supercurrent through the barrier between the two condensates, as illustrated in Figs. 2(f) and 2(g).

Next, we take the hole tunneling as an example to derive this charged current in the excitonic Josephson junctions. The Hamiltonian of the junctions has the form  $\mathcal{H}_{\text{EJJ}} = \mathcal{H}_L + \mathcal{H}_R + \mathcal{H}_T$ , where  $\mathcal{H}_{L(R)}$  is expressed as in Eq. (1) for the left (right) exciton condensate, and the tunneling term  $\mathcal{H}_T$  is treated as a perturbation. The current flowing through the barrier is defined as the rate of the hole number, i.e.,  $I(t) = e(\dot{n}_L(t))$ , in the left condensate. In the interaction representation the  $S$ -matrix expansion approach is applied to deal with the tunneling term [60], and the tunneling current is obtained as

$$I(t) = -e \int_{-\infty}^t \left\{ e^{-i\Delta\mu(t-t')} \langle [\Phi(t), \Phi^\dagger(t')] \rangle - e^{i\Delta\mu(t-t')} \langle [\Phi^\dagger(t), \Phi(t')] \rangle + e^{-i\Delta\mu(t+t')} \langle [\Phi(t), \Phi(t')] \rangle - e^{i\Delta\mu(t+t')} \langle [\Phi^\dagger(t), \Phi^\dagger(t')] \rangle \right\} dt', \quad (5)$$

where the operator  $\Phi(t)$  has the expression  $\Phi(t) = \sum_{kk'} \Gamma_{kk'}^* C_{Rk'}^\dagger(t) C_{Lk}(t)$ , with  $C_{Rk}^*$  and  $C_{Lk}$  is the hole creation and annihilation operator in the right and left condensates, respectively, and  $\Delta\mu = \mu_{hL} - \mu_{hR}$ .

From Eq. (5) we see that there are two components of the total hole tunneling currents: One is the normal current expressed by the first two terms in the braces, determined by the Fermi distributions of hole in both sides of the junction. The other is represented by the last two terms and strongly depends on the order parameters of the condensates on both sides, and this is the charged supercurrent.

The charged supercurrent is described by

$$I_s(t) = -2q \text{Im} [e^{-2i\Delta\mu t} \Xi(\Delta\mu)], \quad (6)$$

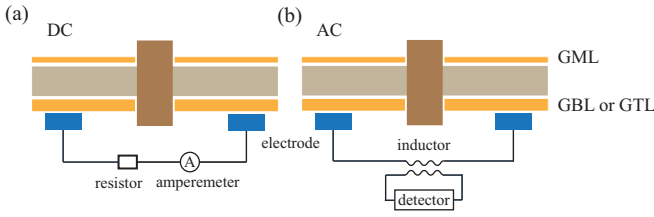


FIG. 3. (a) Schematic diagrams for experimental detection of the single-particle supercurrents in (a) DC and (b) AC regimes.

where  $\Xi(\Delta\mu)$  is the retarded correlation function, and has the expression  $-i \int_0^\infty dt \exp(i\Delta\mu t) \langle [\Phi(t), \Phi(0)] \rangle$ .  $q = -e$  or  $e$  is the charge of the electron or hole carrier. From Eq. (6) we can get the DC or AC nature of the supercurrent by adjusting  $\Delta\mu$ . When  $\Delta\mu$  is small, the electron or hole supercurrent can be obtained by utilizing the macroscopic wave functions of the two constituent exciton condensates, given by  $I_s(t) = 2q\Gamma \sqrt{n_L n_R} \sin(2\Delta\mu t - \Delta\theta)$ , where  $\Delta\theta$  is the phase difference between the two condensates with the corresponding condensate density  $n_{L(R)}$  (see Appendix C).

### C. Potential experimental detection

In experiment the excitonic Josephson junctions can be fabricated with the state-of-the-art technology, such as the multilayer gate technology demonstrated recently in Josephson effects involving magic-angle twisted bilayer graphene [61–63]. Here we propose different approaches to measure experimentally the charged supercurrent based on its DC or AC nature. When the chemical potential difference  $\Delta\mu$  is zero, an electric loop is created to detect the direct supercurrent with a resistor which prevents the quasiparticle current from crossing the barrier, as shown in Fig. 3(a). Such an approach is qualitatively similar to the drag-counterflow geometry proposed earlier for measuring supercurrent in vertically coupled graphene layers [27]. When  $\Delta\mu$  is finite, the supercurrent is of AC nature, accompanied by the noncoherent quasiparticle direct current. Hence the supercurrent can be extracted by an inductor [Fig. 3(b)], and its amplitude and frequency can be obtained as well.

We should point out that the proposed experimental approaches are likely to be somewhat over idealized, and trust the experimental side can readily develop more elegant and ingenious approaches.

Before closing we emphasize that, in the present study, the GML, GBL, and GTL components are adopted to discuss the e-h pair and single particle tunneling regimes in the excitonic Josephson junctions. Conceptually, other 2D materials, such as the transition metal dichalcogenide semiconductors, can also be utilized to realize the charge-neutral or charged supercurrent in an excitonic Josephson junction according to the criterion [Eq. (3) or (4)], thereby broadening the scope and applicability of the main findings made here.

## IV. CONCLUSION

In summary, we have designed excitonic Josephson junctions based on graphene heterostructures, which allows to transit the charge nature of the supercurrent. We have first

examined the constitute condensate systems of an upper GML vertically coupled with a lower GML, GBL, or GTL via a thin h-BN spacer layer, and revealed that the BCS and BKT transition temperatures of such condensates are distinctly influenced by the effective carrier masses. When introducing a barrier between two such identical condensates, a charge-neutral supercurrent has been found to always dominate in the GML/GML scheme, while for the GML/GBL and GML/GTL schemes, a carrier-density induced transition takes place between the charge-neutral and charged supercurrents. In the charged regime, both the electron or hole dominance and DC or AC nature can be tuned by the chemical potential differences of the junction. These findings not only enable direct detection of exciton condensates, offering new opportunities for exploration of their exotic physics, but are also broadly applicable to other excitonic Josephson junctions based on 2D materials beyond graphene.

## ACKNOWLEDGMENTS

This work is supported by the National Key R&D Program of China (Grant No. 2017YFA0303500), the National Natural Science Foundation of China (Grants No. 11974099, No. 11634011, No. 11974323, and No. 11774078), the Fund for Leading Talent in Fundamental Research of the Central China in 2020, the Talents Foundation of Henan Province (CXJD 2021008), and the Anhui Initiative in Quantum Information Technologies (Grant No. AHY170000).

## APPENDIX A: SCREENING EFFECT ON EXCITON ENERGY

In the graphene heterostructures, the densities of electrons and holes can be independently tuned by the electrostatic gates in the upper and lower graphene layers, respectively, and here exciton condensation is considered in the electrically neutral system. For the indirect excitons studied in the present work, we focus on the screened interlayer Coulomb interaction which is written as [45]

$$g(q) = -\frac{2\pi e^2 e^{-qd}}{\epsilon(q + q_{TF} e^{-qd})}, \quad (A1)$$

where  $q$ ,  $\epsilon$ ,  $q_{TF}$ , and  $d$  is the momentum, dielectric constant, Thomas-Fermi momentum, and interlayer distance, respectively. In the above equation, we should pay attention mainly to the term  $q_{TF} e^{-qd}$ , and check its influence on the exciton energy. In GML,  $q_{TF}$  is determined by the carrier density, which implies that the screened Coulomb attraction has the same behavior as the unscreened one, while in GBL or GTL, this physical quantity is directly proportional to the effective mass of the carriers.

For the indirect exciton condensation at low temperature, electrons and holes near the Fermi surfaces in the different layers play the main role, so the Fermi wave vector  $k_F$  can be used to evaluate the screening effect in the Coulomb attraction. Using the parameters in the calculation, we find the screening has a very limited effect on the exciton energy (about 10%).

When further going to the regime of the excitonic Josephson junction, both sides of exciton condensates have the screening effect, and their difference is largely canceled out when the two condensates are close in density, hence the gate-related screening has little influence on the excitonic Josephson effect.

## APPENDIX B: DERIVATION OF THE DISCRIMINANTS II

We start from the Ginzburg-Landau (GL) free energy, which has the form

$$F_{\text{GL}} = -\frac{1}{\beta} \text{Tr} \ln(1 - G_L T G_R T) \approx \frac{1}{\beta} \text{Tr}[G_L T G_R T], \quad (\text{B1})$$

and the physical quantities has the same definitions as those in the main text. When inserting the Green functions into  $F_{\text{GL}}$ , we obtain

$$F_{\text{GL}} = \frac{1}{\beta} \sum_{kk'} \text{tr} \left[ \left( \frac{|\Upsilon_{L1}(k)\rangle\langle\Upsilon_{L1}(k)|T}{i\omega_n - E_{L1}} + \frac{|\Upsilon_{L2}(k)\rangle\langle\Upsilon_{L2}(k)|T}{i\omega_n - E_{L2}} \right) \times \left( \frac{|\Upsilon_{R1}(k')\rangle\langle\Upsilon_{R1}(k')|T}{i\omega_n - E_{R1}} + \frac{|\Upsilon_{R2}(k')\rangle\langle\Upsilon_{R2}(k')|T}{i\omega_n - E_{R2}} \right) \right], \quad (\text{B2})$$

where  $\Upsilon_{\iota\kappa}(k)$  is the wave function of the Bogoliubov–de Gennes Hamiltonian with  $\iota = L$  or  $R$  representing the left or right condensate, and  $\kappa = 1, 2$  for the upper and lower eigenvalues, respectively. After the Matsubara summation, the

GL free energy has the form

$$F_{\text{GL}} = -\frac{1}{2} \sum_{\kappa\kappa'} \text{tr} \left[ \sum_{kk'} \frac{\tanh \frac{\beta E_{L\kappa}}{2} - \tanh \frac{\beta E_{R\kappa'}}{2}}{E_{L\kappa} - E_{R\kappa'}} |\Upsilon_{L\kappa}(k)\rangle \times \langle\Upsilon_{L\kappa}(k)|T| \Upsilon_{R\kappa'}(k')\rangle \langle\Upsilon_{R\kappa'}(k')|T \right]. \quad (\text{B3})$$

Given the wave functions  $\Upsilon_{\iota\kappa}(k)$ ,  $F_{\text{GL}}$  can be obtained, and varies for different tunneling matrices, with the minimum one physically selected. We therefore have the discriminants  $\Pi_e = \min F_{\text{GL}}$  (electron tunneling),  $F_{\text{GL}}$  (e-h tunneling) and  $\Pi_h = \min F_{\text{GL}}$  (hole tunneling),  $F_{\text{GL}}$  (e-h tunneling), as defined in Eqs. (3) and (4) of the main text, when the temperature approaches 0 K.

## APPENDIX C: DERIVATION OF THE EXCITONIC JOSEPHSON CURRENT

To find an expression of the Josephson current  $I_s$ , we take advantage of the macroscopic wave functions of the two constituent exciton condensates, given by  $\Lambda_i = \sqrt{n_i} \exp(i\theta_i)$ , where  $n_i$  and  $\theta_i$  are the condensate density and phase on the left- or right-hand side. The time dependent Schrödinger equations can be applied to discuss the Josephson effect,

$$i \frac{\partial \Lambda_i}{\partial t} = E_i \Lambda_i + \Gamma \Lambda_i. \quad (\text{C1})$$

The supercurrent can be calculated straightforwardly by  $I_s = \pm e \frac{\partial n_i}{\partial t}$  with the corresponding macroscopic wave functions. When the density difference  $|n_L - n_R|$  is small, the time dependence of  $\Delta\theta$  is mainly determined by the energy difference  $(E_R - E_L)$  which is equal to  $-2\Delta\mu$ . Finally, we get the electron or hole supercurrent as shown in the main text.

- 
- [1] J. M. Blatt, K. W. Böer, and W. Brandt, Bose-Einstein condensation of excitons, *Phys. Rev.* **126**, 1691 (1962).
- [2] D. Snoke, Coherent exciton waves, *Science* **273**, 1351 (1996).
- [3] J. P. Eisenstein and A. H. MacDonald, Bose-Einstein condensation of excitons in bilayer electron systems, *Nature (London)* **432**, 691 (2004).
- [4] W. Yao and Q. Niu, Berry Phase Effect on the Exciton Transport and on the Exciton Bose-Einstein Condensate, *Phys. Rev. Lett.* **101**, 106401 (2008).
- [5] R. Anankine, M. Beian, S. Dang, M. Alloing, E. Cambriil, K. Merghem, C. G. Carbonell, A. Lemaître, and F. Dubin, Quantized Vortices and Four-Component Superfluidity of Semiconductor Excitons, *Phys. Rev. Lett.* **118**, 127402 (2017).
- [6] J. R. Leonard, A. A. High, A. T. Hammack, M. M. Fogler, L. V. Butov, K. L. Campman, and A. C. Gossard, Pancharatnam-Berry phase in condensate of indirect excitons, *Nat. Commun.* **9**, 2158 (2018).
- [7] L. V. Butov, A. Zrenner, G. Abstreiter, G. Böhm, and G. Weimann, Condensation of Indirect Excitons in Coupled AlAs/GaAs Quantum Wells, *Phys. Rev. Lett.* **73**, 304 (1994).
- [8] L. V. Butov, A. L. Ivanov, A. Imamoglu, P. B. Littlewood, A. A. Shashkin, V. T. Dolgoplov, K. L. Campman, and A. C. Gossard, Stimulated Scattering of Indirect Excitons in Coupled Quantum Wells: Signature of a Degenerate Bose-Gas of Excitons, *Phys. Rev. Lett.* **86**, 5608 (2001).
- [9] L. V. Butov, C. W. Lai, A. L. Ivanov, A. C. Gossard, and D. S. Chemla, Towards Bose-Einstein condensation of excitons in potential traps, *Nature (London)* **417**, 47 (2002).
- [10] L. V. Butov, A. C. Gossard, and D. S. Chemla, Macroscopically ordered state in an exciton system, *Nature (London)* **418**, 751 (2002).
- [11] L. V. Butov, Condensation of indirect excitons, *MRS Bull.* **45**, 380 (2020).
- [12] A. A. High, J. R. Leonard, A. T. Hammack, M. M. Fogler, L. V. Butov, A. V. Kavokin, K. L. Campman, and A. C. Gossard, Spontaneous coherence in a cold exciton gas, *Nature (London)* **483**, 584 (2012).
- [13] Y. N. Joglekar, A. V. Balatsky, and M. P. Lilly, Excitonic condensate and quasiparticle transport in electron-hole bilayer systems, *Phys. Rev. B* **72**, 205313 (2005).
- [14] B. Wang, J. Peng, D. Y. Xing, and J. Wang, Spin Current Due to Spinlike Andreev Reflection, *Phys. Rev. Lett.* **95**, 086608 (2005).
- [15] M. Rontani and L. J. Sham, Josephson oscillations between exciton condensates in electrostatic traps, *Phys. Rev. B* **80**, 075309 (2009).

- [16] T. Hyart and B. Rosenow, Influence of Topological Excitations on Shapiro Steps and Microwave Dynamical Conductance in Bilayer Exciton Condensates, *Phys. Rev. Lett.* **110**, 076806 (2013).
- [17] C. Zhang and G. Jin, Thermal transport through an exciton-condensate Josephson junction based on graphene double layers, *Appl. Phys. Lett.* **103**, 202111 (2013).
- [18] M. Veldhorst, M. Hoek, M. Snelder, H. Hilgenkamp, A. A. Golubov, and A. Brinkman, Nonlocal spin-entangled Andreev reflection, fractional charge, and current-phase relations in topological bilayer-exciton-condensate junctions, *Phys. Rev. B* **90**, 035428 (2014).
- [19] B. Zenker, H. Fehske, and H. Beck, Excitonic Josephson effect in double-layer graphene junctions, *Phys. Rev. B* **92**, 081111(R) (2015).
- [20] K. S. Novoselov, A. K. Geim, S. V. Morozov, D. Jiang, Y. Zhang, S. V. Dubonos, I. V. Grigorieva, and A. A. Firsov, Electric field effect in atomically thin carbon films, *Science* **306**, 666 (2004).
- [21] K. S. Novoselov, D. Jiang, F. Schedin, T. J. Booth, V. V. Khotkevich, S. V. Morozov, and A. K. Geim, Two-dimensional atomic crystals, *Proc. Natl. Acad. Sci. USA* **102**, 10451 (2005).
- [22] J. N. Coleman, M. Lotya, A. ÓNeill, S. D. Bergin, P. J. King, U. Khan, K. Young, A. Gaucher, S. De, R. J. Smith, I. V. Shvets, S. K. Arora, G. Stanton, H.-Y. Kim, K. Lee, G. T. Kim, G. S. Duesberg, T. Hallam, J. J. Boland, J. J. Wang, J. F. Donegan *et al.*, Two-dimensional nanosheets produced by liquid exfoliation of layered materials, *Science* **331**, 568 (2011).
- [23] Y. Zhan, Z. Liu, S. Najmaei, P. M. Ajayan, and J. Lou, Large-area vapor-phase growth and characterization of MoS<sub>2</sub> atomic layers on a SiO<sub>2</sub> substrate, *Small* **8**, 966 (2012).
- [24] J. H. Choi, P. Cui, H. P. Lan, and Z. Y. Zhang, Linear Scaling of the Exciton Binding Energy Versus the Band Gap of Two-Dimensional Materials, *Phys. Rev. Lett.* **115**, 066403 (2015).
- [25] G. Wang, A. Chernikov, M. M. Glazov, T. F. Heinz, X. Marie, T. Amand, and B. Urbaszek, Excitons in atomically thin transition metal dichalcogenides, *Rev. Mod. Phys.* **90**, 021001 (2018).
- [26] C.-H. Zhang and Y. N. Joglekar, Excitonic condensation of massless fermions in graphene bilayers, *Phys. Rev. B* **77**, 233405 (2008).
- [27] J.-J. Su and A. H. MacDonald, How to make a bilayer exciton condensate flow, *Nat. Phys.* **4**, 799 (2008).
- [28] B. Seradjeh, H. Weber, and M. Franz, Vortices, Zero Modes, and Fractionalization in the Bilayer-Graphene Exciton Condensate, *Phys. Rev. Lett.* **101**, 246404 (2008).
- [29] M. P. Mink, H. T. C. Stoof, R. A. Duine, and A. H. MacDonald, Influence of remote bands on exciton condensation in double-layer graphene, *Phys. Rev. B* **84**, 155409 (2011).
- [30] M. M. Fogler, L. V. Butov, and K. S. Novoselov, High-temperature superfluidity with indirect excitons in van der Waals heterostructures, *Nat. Commun.* **5**, 4555 (2014).
- [31] C. Zhang, W. Zhang, and G. Jin, Floquet exciton condensation in graphene bilayers, *Phys. Rev. B* **92**, 085414 (2015).
- [32] J. I. A. Li, T. Taniguchi, K. Watanabe, J. Hone, and C. R. Dean, Excitonic superfluid phase in double bilayer graphene, *Nat. Phys.* **13**, 751 (2017).
- [33] A. Kogar, M. S. Rak, S. Vig, A. A. Husain, F. Flicker, Y. I. Joe, L. Venema, G. J. MacDougall, T. C. Chiang, E. Fradkin, J. van Wezel, and P. Abbamonte, Signatures of exciton condensation in a transition metal dichalcogenide, *Science* **358**, 1314 (2017).
- [34] P. L. Ríos, A. Perali, R. J. Needs, and D. Neilson, Evidence from Quantum Monte Carlo Simulations of Large-Gap Superfluidity and BCS-BEC Crossover in Double Electron-Hole Layers, *Phys. Rev. Lett.* **120**, 177701 (2018).
- [35] Z. Jiang, W. Lou, Y. Liu, Y. Li, H. Song, K. Chang, W. Duan, and S. Zhang, Spin-Triplet Excitonic Insulator: The Case of Semihydrogenated Graphene, *Phys. Rev. Lett.* **124**, 166401 (2020).
- [36] Z. Wang, D. A. Rhodes, K. Watanabe, T. Taniguchi, J. C. Hone, J. Shan, and K. F. Mak, Evidence of high-temperature exciton condensation in two-dimensional atomic double layers, *Nature (London)* **574**, 76 (2019).
- [37] L. Britnell, R. V. Gorbachev, R. Jalil, B. D. Belle, F. Schedin, A. Mishchenko, T. Georgiou, M. I. Katsnelson, L. Eaves, S. V. Morozov, N. M. R. Peres, J. Leist, A. K. Geim, K. S. Novoselov, and L. A. Ponomarenko, Field-effect tunneling transistor based on vertical graphene heterostructures, *Science* **335**, 947 (2012).
- [38] T. Georgiou, R. Jalil, B. D. Belle, L. Britnell, R. V. Gorbachev, S. V. Morozov, Y.-J. Kim, A. Gholinia, S. J. Haigh, O. Makarovsky, L. Eaves, L. A. Ponomarenko, A. K. Geim, K. S. Novoselov, and A. Mishchenko, Vertical field-effect transistor based on graphene-WS<sub>2</sub> heterostructures for flexible and transparent electronics, *Nat. Nanotech.* **8**, 100 (2013).
- [39] G. W. Burg, N. Prasad, K. Kim, T. Taniguchi, K. Watanabe, A. H. MacDonald, L. F. Register, and E. Tutuc, Strongly Enhanced Tunneling at Total Charge Neutrality in Double-Bilayer Graphene-WSe<sub>2</sub> Heterostructures, *Phys. Rev. Lett.* **120**, 177702 (2018).
- [40] J. Stajic, FFLO on the horizon, *Science* **330**, 429 (2010).
- [41] K. B. Gubbels, M. W. J. Romans, and H. T. C. Stoof, Sarma Phase in Trapped Unbalanced Fermi Gases, *Phys. Rev. Lett.* **97**, 210402 (2006).
- [42] M. I. Katsnelson, K. S. Novoselov, and A. K. Geim, Chiral tunnelling and the Klein paradox in graphene, *Nat. Phys.* **2**, 620 (2006).
- [43] A. F. Young and P. Kim, Quantum interference and Klein tunnelling in graphene heterojunctions, *Nat. Phys.* **5**, 222 (2009).
- [44] N. Stander, B. Huard, and D. Goldhaber-Gordon, Evidence for Klein Tunneling in Graphene *p-n* Junctions, *Phys. Rev. Lett.* **102**, 026807 (2009).
- [45] V. N. Kotov, B. Uchoa, V. M. Pereira, F. Guinea, and A. H. Castro Neto, Electron-electron interactions in graphene: Current status and perspectives, *Rev. Mod. Phys.* **84**, 1067 (2012).
- [46] S. De Palo, F. Rapisarda, and G. Senatore, Excitonic Condensation in a Symmetric Electron-Hole Bilayer, *Phys. Rev. Lett.* **88**, 206401 (2002).
- [47] D. V. Khveshchenko, Ghost Excitonic Insulator Transition in Layered Graphite, *Phys. Rev. Lett.* **87**, 206401 (2001).
- [48] R. Maezono, P. L. Ríos, T. Ogawa, and R. J. Needs, Excitons and Biexcitons in Symmetric Electron-Hole Bilayers, *Phys. Rev. Lett.* **110**, 216407 (2013).
- [49] D. Snoke, Spontaneous Bose coherence of excitons and polaritons, *Science* **298**, 1368 (2002).
- [50] J. M. Kosterlitz and D. J. Thouless, Ordering, metastability, and phase transitions in two-dimensional systems, *J. Phys. C: Solid State Phys.* **6**, 1181 (1973).
- [51] D. J. Scalapino, S. R. White, and S. C. Zhang, Insulator, metal, or superconductor: The criteria, *Phys. Rev. B* **47**, 7995 (1993).

- [52] L. Liang, T. I. Vanhala, S. Peotta, T. Siro, A. Harju, and P. Törmä, Band geometry, Berry curvature, and superfluid weight, *Phys. Rev. B* **95**, 024515 (2017).
- [53] X. Hu, T. Hyart, D. I. Pikulin, and E. Rossi, Geometric and Conventional Contribution to the Superfluid Weight in Twisted Bilayer Graphene, *Phys. Rev. Lett.* **123**, 237002 (2019).
- [54] M. P. Mink, H. T. C. Stoof, R. A. Duine, M. Polini, and G. Vignale, Probing the Topological Exciton Condensate via Coulomb Drag, *Phys. Rev. Lett.* **108**, 186402 (2012).
- [55] L. Zhu, L. Li, R. Tao, X. Fan, X. Wan, and C. Zeng, Frictional drag effect between massless and massive fermions in single-layer/bilayer graphene heterostructures, *Nano Lett.* **20**, 1396 (2020).
- [56] B. D. Josephson, Possible new effects in superconductive tunnelling, *Phys. Lett.* **1**, 251 (1962).
- [57] P. W. Anderson and J. M. Rowell, Probable Observation of the Josephson Superconducting Tunneling Effect, *Phys. Rev. Lett.* **10**, 230 (1963).
- [58] E. K. Dahl and A. Sudbø, Derivation of the Ginzburg-Landau equations for a ferromagnetic  $p$ -wave superconductor, *Phys. Rev. B* **75**, 144504 (2007).
- [59] Q. Sun, Z. Jiang, Y. Yu, and X. C. Xie, Spin superconductor in ferromagnetic graphene, *Phys. Rev. B* **84**, 214501 (2011).
- [60] G. D. Mahan, *Many-Particle Physics* (Kluwer Academic/Plenum, New York, 2000).
- [61] D. Rodan-Legrain, Y. Cao, J. M. Park, S. C. de la Barrera, M. T. Randeria, K. Watanabe, T. Taniguchi, and P. Jarillo-Herrero, Highly tunable junctions and non-local Josephson effect in magic-angle graphene tunnelling devices, *Nat. Nanotechnol.* **16**, 769 (2021).
- [62] F. K. de Vries, E. Portolés, G. Zheng, T. Taniguchi, K. Watanabe, T. Ihn, K. Ensslin, and P. Rickhaus, Gate-defined Josephson junctions in magic-angle twisted bilayer graphene, *Nat. Nanotechnol.* **16**, 760 (2021).
- [63] E. D. Walsh, W. Jung, G.-H. Lee, D. K. Efetov, B.-I. Wu, K.-F. Huang, T. A. Ohki, T. Taniguchi, K. Watanabe, P. Kim, D. Englund, and K. C. Fong, Josephson junction infrared single-photon detector, *Science* **372**, 409 (2021).